Wireless Netw (2012) 18:735–747
DOI 10.1007/s11276-012-0429-0

Derivation of CRLB for linear least square estimator in wireless location systems

Po-Hsuan Tseng · Kai-Ten Feng

Published online: 18 March 2012

Abstract Linear estimators, including the well-adopted linear least squares (LLS) estimator, have been extensively utilized for wireless location estimation for their simplicity and closed-form property. However, there exists information lost from the linearization of the location estimator to the nonlinear location estimation, which prevents the linear estimator from approaching the Cramer-Rao lower bound (CRLB). In this paper, the linearized location estimation problem based CRLB (L-CRLB) is derived to provide a portrayal in order to fully characterize the behavior of the linearized location estimator. The relationships between the L-CRLB and the CRLB are obtained and theoretically proven in this paper. Furthermore, the geometric layout between the mobile station (MS) and the base stations (BSs) that can achieve the minimum L-CRLB is also acquired. As can be suggested by the L-CRLB, an LLS location estimator can achieve higher accuracy if the MS is located inside the geometry confined by the BSs compared to the case that the MS is situated outside of the geometric layout. This result will be beneficial to the deployment of BSs or the signal selection schemes targeting for location estimation. Simulation results utilizing the LLS estimator as one of the implementation of the linearized location estimators further validate the theoretical proofs and the effectiveness of the L-CRLB.

Keywords Linear least square (LLS) estimator · Cramèr-Rao lower bound (CRLB)

P.-H. Tseng · K.-T. Feng (✉)
Department of Electrical Engineering,
National Chiao Tung University, Hsinchu, Taiwan
e-mail: ktfeng@mail.nctu.edu.tw

P.-H. Tseng
e-mail: walker.cm90@nctu.edu.tw

1 Introduction

Wireless location technologies, which are designated to estimate the position of a mobile station (MS), have drawn a lot of attention over the past few decades. The quality-of-service (QoS) of positioning accuracy has been announced after the issue of emergency 911 (E-911) subscriber safety service [1]. With the assistance of information derived from the positioning system, the required performance and objectives for the targeting MS can be achieved with augmented robustness. In recent years, there are increasing demands for commercial applications to adopt the location information within their system design, such as the navigation systems, the location-based billing, the health care systems, the wireless sensor networks (WSNs) [2–4] and the intelligent transportation systems (ITSs) [5, 6]. With emergent interests in the location-based services (LBSs) [7], location estimation algorithms with enhanced precision become necessitate for the applications under different circumstances.

The location estimation schemes [8, 9] have been widely proposed and employed in the wireless communication system. These schemes locate the position of an MS based on the measured radio signals from its neighborhood base stations (BSs). The representative distance measurements for the wireless location estimation techniques are the time-of-arrival (TOA), the time difference-of-arrival (TDOA), and the angle-of-arrival (AOA). The TOA scheme measures the arrival time of radio signals coming from different wireless BSs; while the TDOA scheme measures the time difference between the radio signals. The AOA technique is conducted within the BS by observing the arriving angle of signals coming from the MS. The TOA measurement is discussed in the paper. However, it is recognized that the equations associated with the TOA estimation schemes are inherently nonlinear. The uncertainties induced by the

measurement noises make it more difficult to acquire the MS's estimated position with tolerable precision.

There are several representative techniques which are widely utilized in practical localization systems, such as the Taylor series expansion (TSE) based method, the fingerprinting method, and the linear least squares (LLS) method. The TSE method utilized in [10] requires iterative processes to obtain the location estimate from another linearized system based on the Taylor series expansion. The major drawback of the TSE method is that it may suffer from the convergence problem due to an incorrect initial guess of the MS's position. The pattern-matching localization based on the fingerprinting approach is another popular method for the LEP, e.g., RADAR [11]. However, a large amount of measurements are required to be collected from a database before the estimation. The LLS [12] is one of the popular techniques adopted in practical localization systems, e.g., the Cricket system [13], and has been continuously investigated from research perspectives [14–17]. By introducing an additional variable, the LLS scheme can transform the original nonlinear estimation problem into a linear relationship for the computation of MS's position. Moreover, the closed-form characteristic of LLS estimator is suitable for real-time implementation due to its computation efficiency.

The location estimator discussed in this paper belongs to non-Bayesian approach, i.e., without a priori knowledge of the parameter. The Cramer-Rao lower bound (CRLB) [18, 19] serves as a benchmark of the non-Bayesian estimator. An estimator that can achieve the CRLB under regularity conditions is the maximum likelihood (ML) estimator. The CRLB for the conventional location estimation problem (LEP) is derived in [19]. Since the wireless location estimation schemes are inherently nonlinear, the original LEP is often transformed into a linearized location estimation problem (L-LEP) by introducing an additional variable to transfer the nonlinear equation into a linear equation for the computation of MS's position in practice. This transformation leads to a different parameterization and the analysis of the L-LEP has not been fully addressed in the previous research work.

Based on the concept of the CRLB, the theoretic lower bound of the L-LEP is derived as the L-LEP based CRLB (L-CRLB) in the paper. The major target of this paper is to derive the L-CRLB as a new performance metric for the LLS estimator and also observes the geometric properties associated with the proposed L-CRLB. The closed-forms formulation of the Fisher information matrix (FIM) for the derived L-CRLB provides a comparison between the L-LEP and the conventional LEP. Since it is required for the L-LEP to estimate an additional variable other than the MS's position, it can be proved that the value of L-CRLB is greater than or equal to the conventional CRLB. The geometric layout between the MS and the BSs for the L-CRLB to be equivalent to the CRLB is also derived.

Note that the LLS method is one of the methods to solve the L-LEP. In the paper, the unbiased property of the LLS estimator is proven under the situation that the noiseless distance is much greater than the combined noise for each measurement. Besides, the LLS method becomes a ML estimator in a linear problem when the noise is assumed to be Gaussian distributed. It is validated in the simulations that the L-CRLB can be served as a tight lower bound for the mean square error of the LLS estimator. Therefore, the L-CRLB can be adopted as the benchmark of LLS estimator and all the properties of L-CRLB derived in the paper will be feasible to characterize the behaviors of LLS estimator. From the geometric point of view, it can be inferred from the proposed L-CRLB that the LLS estimator will provide better performance if the MS is located inside the geometry constrained by the BSs; while inferior performance is acquired if the MS is outside of the geometric layout. This result can also be validates by the observations as was simulated in [12]. By adopting the proposed L-CRLB under different geometric layouts, the LLS estimator can be regarded as an efficient estimator while the MS is located within the geometry formed by the BSs. This observation will be beneficial for the signal selection schemes of measurement inputs which should try to avoid positioning the signal sources that makes the MS to locate outside of the geometric layout.

The remainder of this paper is organized as follows. Section 2 describes the modeling and geometric properties of both the CRLB and the L-CRLB. The realization of the LLS estimator for the L-LEP and the situation that the LLS estimator is unbiased are presented in Sect. 3. Section 4 illustrates the performance validation and evaluation for the both the proposed L-CRLB and the LLS estimator. Section 5 draws the conclusion.

2 Analysis of CRLB and L-CRLB

2.1 Mathematical modeling of signal sources

The signal model for the TOA measurements is utilized for two-dimension (2-D) location estimation. The set $\boldsymbol{r}$ contains all the available measured relative distance, i.e., $\boldsymbol{r} = [r_1, \ldots, r_i, \ldots, r_N]$ where N denotes the number of available BSs. The measured relative distance between the MS and the i-th BS can be represented as

$$r_i = c \cdot t_i = \zeta_i + n_i \qquad \text{for } i = 1, 2, \ldots, N \tag{1}$$

where c is the speed of light. The parameter t_i indicates the TOA measurement obtained from the i-th BS, which is contaminated with the measurement noise n_i. The noiseless

relative distance ζ_i in (1) between the MS's true position and the i-th BS can be acquired as

$$\zeta_i = \|\boldsymbol{x} - \boldsymbol{x}_i\| \qquad \text{for } i = 1, 2, \ldots, N \tag{2}$$

where $\boldsymbol{x} = [x, y]^T$ represents the MS's true position and $\boldsymbol{x}_i = [x_i, y_i]^T$ is the location of the i-th BS. The notations $\|.\|$ denotes the Euclidean norm of a vector and $[.]^T$ represents the transpose operator.

Definition 1 (*BS's Orientation*) Considering the MS as a vertex in geometry, the orientation of i-th BS (α_i) is defined as the angle between the MS to the i-th BS and the positive x axis. Without loss of generality, the index i of BSs are sorted such that the i-th BS is located at the angle $\alpha_1 \le \alpha_2 \le \ldots \alpha_i \ldots \le \alpha_N$ for $i = 1$ to N.

Based on the definition of α_i, the following geometric relationship can also be obtained as $\cos\alpha_i = (x_i - x)/\zeta_i$ and $\sin\alpha_i = (y_i - y)/\zeta_i$.

2.2 Properties of CRLB

Definition 2 (*Location Estimation Problem (LEP)*) By collecting the measurements $\boldsymbol{r}$, the goal of the LEP is to generate a 2-D estimate $\hat{\boldsymbol{x}} = [\hat{x}, \hat{y}]^T$ of the MS's location.

The CRLB represents the theoretical lowest error variance of an unknown parameter for any unbiased estimator. Note that the CRLB in the rest of this paper refers to the CRLB for the conventional LEP. Therefore, based on the TOA-based LEP as in (1) and (2), the variance of the MS's estimated position $\hat{\boldsymbol{x}}$ will be greater or equal to the CRLB ($\mathcal{C}$) as

$$E\{\|\hat{\boldsymbol{x}} - \boldsymbol{x}\|^2\} \ge \mathcal{C} = [\mathbf{I}_{\boldsymbol{x}}^{-1}]_{11} + [\mathbf{I}_{\boldsymbol{x}}^{-1}]_{22} \tag{3}$$

where the CRLB $\mathcal{C} = [\mathbf{I}_{\boldsymbol{x}}^{-1}]_{11} + [\mathbf{I}_{\boldsymbol{x}}^{-1}]_{22}$ inherently represents the theoretical minimum mean square error (MMSE) of position. It is noted that $[\mathbf{I}_{\boldsymbol{x}}^{-1}]_{11}$ and $[\mathbf{I}_{\boldsymbol{x}}^{-1}]_{22}$ correspond to the first and second diagonal terms of the inverse of 2×2 FIM $\mathbf{I}_{\boldsymbol{x}}$, which can be obtained as

$$\mathbf{I}_{\boldsymbol{x}} = \mathbf{G} \cdot \mathbf{I}_{\boldsymbol{\zeta}} \cdot \mathbf{G}^T \tag{4}$$

where

$$\mathbf{G} = \frac{\partial \boldsymbol{\zeta}}{\partial \boldsymbol{x}} = \begin{bmatrix} \frac{x_1 - x}{\zeta_1} & \ldots & \frac{x_i - x}{\zeta_i} & \ldots & \frac{x_N - x}{\zeta_N} \\ \frac{y_1 - y}{\zeta_1} & \ldots & \frac{y_i - y}{\zeta_i} & \ldots & \frac{y - y_N}{\zeta_N} \end{bmatrix} = \begin{bmatrix} \cos\alpha_1 & \ldots & \cos\alpha_i & \ldots & \cos\alpha_N \\ \sin\alpha_1 & \ldots & \sin\alpha_i & \ldots & \sin\alpha_N \end{bmatrix} \tag{5}$$

$$\mathbf{I}_{\boldsymbol{\zeta}} = E\left[\frac{\partial}{\partial \boldsymbol{\zeta}} \ln f(\boldsymbol{r}|\boldsymbol{\zeta}) \cdot \left(\frac{\partial}{\partial \boldsymbol{\zeta}} \ln f(\boldsymbol{r}|\boldsymbol{\zeta})\right)^T\right] \tag{6}$$

The $f(\boldsymbol{r}|\boldsymbol{\zeta})$ function in (6) denotes the probability density function for $\boldsymbol{r}$ conditioning on $\boldsymbol{\zeta}$, where $\boldsymbol{\zeta} = [\zeta_1, \ldots, \zeta_i, \ldots, \zeta_N]$. The matrices $\mathbf{G}$ and $\mathbf{I}_{\boldsymbol{\zeta}}$ are introduced as the change of variables since $\mathbf{I}_{\boldsymbol{x}}$ is unobtainable owing to the unknown MS's true position $\boldsymbol{x}$.

Lemma 1 *Considering the TOA-based LEP, the noise model for each measurement r_i is an i.i.d. Gaussian distribution with zero mean and a fixed set of variances σ_{ri}^2 as $n_i \sim \mathcal{N}(0, \sigma_{r_i}^2)$. The minimum CRLB $\mathcal{C}_m$ with respect to the angle α_i can be achieved in* [19] *as*

$$\mathcal{C}_m = \frac{4}{\sum_{i=1}^{N} \frac{1}{\sigma_{r_i}^2}} \tag{7}$$

if the following two conditions hold:

$$\begin{cases} \sum_{i=1}^{N} \frac{1}{\sigma_{r_i}^2} \sin 2\alpha_i = 0 \\ \sum_{i=1}^{N} \frac{1}{\sigma_{r_i}^2} \cos 2\alpha_i = 0 \end{cases} \tag{8}$$

Proof Based on (1), $f(\boldsymbol{r}|\boldsymbol{\zeta})$ can be obtained as

$$f(\boldsymbol{r}|\boldsymbol{\zeta}) \propto \prod_{i=1}^{N} \exp\left[-\frac{1}{2\sigma_{r_i}^2}(r_i - \zeta_i)^2\right] \tag{9}$$

Therefore, the matrix $\mathbf{I}_{\boldsymbol{\zeta}}$ can be derived from (6) as $\mathbf{I}_{\boldsymbol{\zeta}} = \text{diag}\{[\sigma_{r_1}^{-2}, \sigma_{r_2}^{-2}, \ldots, \sigma_{r_i}^{-2}, \ldots, \sigma_{r_N}^{-2}]\}$. The 2×2 matrix $\mathbf{I}_{\boldsymbol{x}}$ can be obtained from (4) and (6) as

$$\mathbf{I}_{\boldsymbol{x}} = \begin{bmatrix} [\mathbf{I}_{\boldsymbol{x}}]_{11} & [\mathbf{I}_{\boldsymbol{x}}]_{12} \\ [\mathbf{I}_{\boldsymbol{x}}]_{21} & [\mathbf{I}_{\boldsymbol{x}}]_{22} \end{bmatrix} = \begin{bmatrix} \sum_{i=1}^{N} \frac{1}{\sigma_{r_i}^2} \cos^2\alpha_i & \sum_{i=1}^{N} \frac{1}{\sigma_{r_i}^2} \cos\alpha_i \cdot \sin\alpha_i \\ \sum_{i=1}^{N} \frac{1}{\sigma_{r_i}^2} \cos\alpha_i \cdot \sin\alpha_i & \sum_{i=1}^{N} \frac{1}{\sigma_{r_i}^2} \sin^2\alpha_i \end{bmatrix} \tag{10}$$

In order to obtain the minimum CRLB, (3) can further be derived as

$$E\{(\hat{\boldsymbol{x}} - \boldsymbol{x})^2\} \ge [\mathbf{I}_{\boldsymbol{x}}^{-1}]_{11} + [\mathbf{I}_{\boldsymbol{x}}^{-1}]_{22} = \frac{[\mathbf{I}_{\boldsymbol{x}}]_{11} + [\mathbf{I}_{\boldsymbol{x}}]_{22}}{[\mathbf{I}_{\boldsymbol{x}}]_{11} \cdot [\mathbf{I}_{\boldsymbol{x}}]_{22} - [\mathbf{I}_{\boldsymbol{x}}]_{12}^2} \ge \frac{[\mathbf{I}_{\boldsymbol{x}}]_{11} + [\mathbf{I}_{\boldsymbol{x}}]_{22}}{[\mathbf{I}_{\boldsymbol{x}}]_{11} \cdot [\mathbf{I}_{\boldsymbol{x}}]_{22}} \tag{11}$$

Noted that the second inequality in (11) is valid since the quadratic term $[\mathbf{I}_{\boldsymbol{x}}]_{12}^2 \ge 0$ for all α_i. Therefore, one of the necessary conditions to achieve minimum CRLB will be $[\mathbf{I}_{\boldsymbol{x}}]_{12} = \sum_{i=1}^{N} \frac{1}{\sigma_{r_i}^2} \cos\alpha_i \cdot \sin\alpha_i = 0$, which validates the first equation of (8). Moreover, since $\cos^2\alpha_i + \sin^2\alpha_i = 1$ for all α_i, the numerator in (11) becomes $[\mathbf{I}_{\boldsymbol{x}}]_{11} + [\mathbf{I}_{\boldsymbol{x}}]_{22} = \sum_{i=1}^{N} 1/\sigma_{r_i}^2$. Consequently, to acquire the minimum value of CRLB corresponds to maximizing the denominator $[\mathbf{I}_{\boldsymbol{x}}]_{11} \cdot [\mathbf{I}_{\boldsymbol{x}}]_{22}$ in (11). According to the *inequality of arithmetic and geometric means*, the following relationship can be obtained:

$$\sqrt{[\mathbf{I}_{\boldsymbol{x}}]_{11} \cdot [\mathbf{I}_{\boldsymbol{x}}]_{22}} \le \frac{[\mathbf{I}_{\boldsymbol{x}}]_{11} + [\mathbf{I}_{\boldsymbol{x}}]_{22}}{2} = \frac{1}{2} \sum_{i=1}^{N} \frac{1}{\sigma_{r_i}^2} \tag{12}$$

where the equality holds if and only if $[\mathbf{I}_x]_{11} = [\mathbf{I}_x]_{22}$, which corresponds to the second equation in (8). By substituting (12) into (11), the minimum CRLB can be obtained as $\mathcal{C}_m = 4/(\sum_{i=1}^{N} \frac{1}{\sigma_{r_i}^2})$. This completes the proof. □

Example 1 (Network Layout with Minimum CRLB). Following the requirement as in Lemma 1 with $N = 3$ and all the variances are equivalent $\sigma_{ri}^2 = \sigma_r^2$ for $i = 1$ to 3, the best geometric layout that can achieve the minimum CRLB $\mathcal{C}_m = 4\sigma_r^2/3$ is acquired at either the angle sets $\{\alpha_1, \alpha_2, \alpha_3\} = \{\gamma, \gamma + 120°, \gamma + 240°\}$ or $\{\alpha_1, \alpha_2, \alpha_3\} = \{\gamma, \gamma + 60°, \gamma + 120°\}$ $\forall\ \gamma = [0°, 360°)$.

2.3 Properties of proposed L-CRLB

Definition 3 (*Linearized Location Estimation Problem (L-LEP)*). In order to estimate the MS's position $\boldsymbol{x}$, the nonlinear terms x^2 and y^2 in (2) are replaced by a new parameter $R = x^2 + y^2$. The goal of the L-LEP is to generate an estimate $\hat{\boldsymbol{\theta}} = [\hat{x}_L, \hat{y}_L, \hat{R}]^T$ based on the collecting measurements $\boldsymbol{r}$.

Note that the MS's estimated position $\hat{\boldsymbol{x}}_L = [\hat{x}_L, \hat{y}_L]^T$ of the L-LEP is in general not optimal compared to the original LEP since an additional nonlinear parameter R is also estimated, which reduces the estimation precision for $\hat{\boldsymbol{x}}_L$ under fixed set of measurement inputs. This intuitive observation explains that the conventional CRLB cannot be achieved by the linearized location estimator for LEP. In order to appropriately describe the behavior of linearized location estimator, the L-CRLB is defined based on the relationships in (1) and (2) as follows.

Definition 4 (*L-CRLB*) The L-CRLB ($\mathcal{C}_L$) is defined for linearized location estimation in terms of the estimated parameters $\hat{\boldsymbol{x}}_L$ as

$$E\{\|\hat{\boldsymbol{x}}_L - \boldsymbol{x}\|^2\} \geq \mathcal{C}_L = [\mathbf{I}_{\boldsymbol{\theta}}^{-1}]_{11} + [\mathbf{I}_{\boldsymbol{\theta}}^{-1}]_{22} \tag{13}$$

where $[\mathbf{I}_{\boldsymbol{\theta}}^{-1}]_{11}$ and $[\mathbf{I}_{\boldsymbol{\theta}}^{-1}]_{22}$ respectively denotes the first and second diagonal terms of the inverse of 3×3 FIM matrix $\mathbf{I}_{\boldsymbol{\theta}}$ as

$$\mathbf{I}_{\boldsymbol{\theta}} = \mathbf{H} \cdot \mathbf{I}_{\boldsymbol{\zeta}} \cdot \mathbf{H}^T \tag{14}$$

with

$$\mathbf{H} = \frac{\partial \boldsymbol{\zeta}}{\partial \boldsymbol{\theta}} = \begin{bmatrix} \cos\alpha_1 & \cdots & \cos\alpha_i & \cdots & \cos\alpha_N \\ \sin\alpha_1 & \cdots & \sin\alpha_i & \cdots & \sin\alpha_N \\ \frac{1}{2\zeta_1} & \cdots & \frac{1}{2\zeta_i} & \cdots & \frac{1}{2\zeta_N} \end{bmatrix} \tag{15}$$

and $\mathbf{I}_{\boldsymbol{\zeta}}$ obtained from (6).

Note that the derivation of the inequality (13) is neglected in this paper, which can be similarly referred from the derivation of CRLB in [20]. Based on the theory of CRLB, the closed-forms of FIM in (14) can be formulated and the relevant matrix in (15) is derived. In other words, the proposed L-CRLB is utilized to denote the minimum variance for any estimator that estimates the parameter vector $\boldsymbol{\theta}$ from the TOA measurements. In the following lemma, the fact that the L-CRLB is greater than or equal to the CRLB will be proved.

Lemma 2 *Considering that there exists sufficient measurement inputs for location estimation with zero mean Gaussian noises, the L-CRLB is greater than or equal to the CRLB, i.e.,* $\mathcal{C}_L \geq \mathcal{C}$.

Proof The 3×3 matrix $\mathbf{I}_{\boldsymbol{\theta}}$ can be obtained from (6) and (14) as

$$\mathbf{I}_{\boldsymbol{\theta}} = \begin{bmatrix} \mathbf{I}_x & \mathbf{B} \\ \mathbf{B}^T & \mathbf{C} \end{bmatrix} = \begin{bmatrix} \sum_{i=1}^{N} \frac{1}{\sigma_{r_i}^2}\cos^2\alpha_i & \sum_{i=1}^{N} \frac{1}{\sigma_{r_i}^2}\cos\alpha_i \cdot \sin\alpha_i & \sum_{i=1}^{N} \frac{1}{\sigma_{r_i}^2}\frac{\cos\alpha_i}{2\zeta_i} \\ \sum_{i=1}^{N} \frac{1}{\sigma_{r_i}^2}\cos\alpha_i \cdot \sin\alpha_i & \sum_{i=1}^{N} \frac{1}{\sigma_{r_i}^2}\sin^2\alpha_i & \sum_{i=1}^{N} \frac{1}{\sigma_{r_i}^2}\frac{\sin\alpha_i}{2\zeta_i} \\ \sum_{i=1}^{N} \frac{1}{\sigma_{r_i}^2}\frac{\cos\alpha_i}{2\zeta_i} & \sum_{i=1}^{N} \frac{1}{\sigma_{r_i}^2}\frac{\sin\alpha_i}{2\zeta_i} & \sum_{i=1}^{N} \frac{1}{4\sigma_{r_i}^2\zeta_i^2} \end{bmatrix} \tag{16}$$

where the matrices $\mathbf{B} = \left[\sum_{i=1}^{N} \frac{1}{\sigma_{r_i}^2}\frac{\cos\alpha_i}{2\zeta_i} \ \sum_{i=1}^{N} \frac{1}{\sigma_{r_i}^2}\frac{\sin\alpha_i}{2\zeta_i}\right]^T$ and $\mathbf{C} = \left[\sum_{i=1}^{N} \frac{1}{4\sigma_{r_i}^2\zeta_i^2}\right]$. Note that the 2×2 matrix $\mathbf{I}_x$ is the same as that obtained from (4). Moreover, the inverse of the covariance matrix $\mathbf{I}_{\boldsymbol{\theta}}$ can be represented as

$$\mathbf{I}_{\boldsymbol{\theta}}^{-1} = \begin{bmatrix} [\mathbf{I}_{\boldsymbol{\theta}}]_{2\times2}^{-1} & \mathbf{B}' \\ \mathbf{B}'^T & \mathbf{C}' \end{bmatrix} \tag{17}$$

where the 2×2 submatrix $[\mathbf{I}_{\boldsymbol{\theta}}]_{2\times2}^{-1}$ of $\mathbf{I}_{\boldsymbol{\theta}}^{-1}$ can be obtained as $[\mathbf{I}_{\boldsymbol{\theta}}]_{2\times2}^{-1} = (\mathbf{I}_x - \mathbf{B} \cdot \mathbf{C}^{-1} \cdot \mathbf{B}^T)^{-1}$ based on the matrix inversion lemma. Considering that there are sufficient measurement inputs for the linearized location estimation, i.e., $N \geq 3$, both the covariance matrices $\mathbf{I}_{\boldsymbol{\theta}}$ and $\mathbf{I}_x$ are non-singular which corresponds to positive definite matrices. Consequently, the submatrix $[\mathbf{I}_{\boldsymbol{\theta}}]_{2\times2}$ and their corresponding inverse matrices $\mathbf{I}_{\boldsymbol{\theta}}^{-1}, \mathbf{I}_x^{-1}$, and $[\mathbf{I}_{\boldsymbol{\theta}}]_{2\times2}^{-1}$ are positive definite. Furthermore, both $\mathbf{C}$ and $\mathbf{C}^{-1}$ are positive definite since $\mathbf{C} = \left[\sum_{i=1}^{N} \frac{1}{4\sigma_{r_i}^2\zeta_i^2}\right] > 0$. Therefore, it can be shown that $[\mathbf{I}_{\boldsymbol{\theta}}]_{2\times2} = (\mathbf{I}_x - \mathbf{B} \cdot \mathbf{C}^{-1} \cdot \mathbf{B}^T) \leq \mathbf{I}_x$ since $\mathbf{C}^{-1}$ is positive definite and the equality only occurs with zero matrix $\mathbf{B}$. Given two positive definite matrices $[\mathbf{I}_{\boldsymbol{\theta}}]_{2\times2}$ and $\mathbf{I}_x, \mathbf{I}_x \geq [\mathbf{I}_{\boldsymbol{\theta}}]_{2\times2}$ if and only if $[\mathbf{I}_{\boldsymbol{\theta}}]_{2\times2}^{-1} \geq \mathbf{I}_x^{-1} > 0$. Furthermore, since $[\mathbf{I}_{\boldsymbol{\theta}}]_{2\times2}^{-1} \geq \mathbf{I}_x^{-1}$, their corresponding traces will follow as $\text{trace}([\mathbf{I}_{\boldsymbol{\theta}}]_{2\times2}^{-1}) \geq \text{trace}(\mathbf{I}_x^{-1})$ which consequently results in $[\mathbf{I}_{\boldsymbol{\theta}}]_{11}^{-1} + [\mathbf{I}_{\boldsymbol{\theta}}]_{22}^{-1} \geq [\mathbf{I}_x]_{11}^{-1} + [\mathbf{I}_x]_{22}^{-1}$. This completes the proof. □

Corollary 1 *The L-CRLB is equivalent to the CRLB if the following two conditions hold*

$$\begin{cases} \sum_{i=1}^{N} \frac{1}{\sigma_{r_i}^2} \frac{\sin \alpha_i}{\zeta_i} = 0 \\ \sum_{i=1}^{N} \frac{1}{\sigma_{r_i}^2} \frac{\cos \alpha_i}{\zeta_i} = 0 \end{cases} \tag{18}$$

Proof As stated in Lemma 2, the necessary and sufficient condition for both L-CRLB and CRLB to be equivalent is that **B** is a zero matrix. Therefore, the two matrix elements in **B**, i.e., $\sum_{i=1}^{N} \cos \alpha_i/(\sigma_{r_i}^2 \zeta_i)$ and $\sum_{i=1}^{N} \sin \alpha_i/(\sigma_{r_i}^2 \zeta_i)$, will be equal to zero. □

It can be generalized from Corollary 1 that the two error terms $\varepsilon_1 = \sum_{i=1}^{N} \cos \alpha_i/(\sigma_{r_i}^2 \zeta_i)$ and $\varepsilon_2 = \sum_{i=1}^{N} \sin \alpha_i/(\sigma_{r_i}^2 \zeta_i)$ will influence the value of L-CRLB, which consequently affect the precision of linearized location estimators. Under the geometric layout with smaller values of ε_1 and ε_2, smaller difference between the CRLB and L-CRLB value can be obtained, which indicates that the linearization lost by adopting linearized location estimators is smaller. ε_1 and ε_2 can be mapping to the x- and y-direction vectors from the MS to the BS. The noise variance terms can be regarded as the weighting of the direction vector. The minimum linearization lost for the linearized location estimator is achieved when the sum of the weighted direction vector from the MS to the BS is equal to zero. Besides, consider the case that the MS is situated outside of the polygon formed by the BSs, all the angles α_i will be in the range of [0, 180°] which results in larger value of the error terms ε_1 and ε_2. As a result, the estimation errors acquired from the linearized location estimator will be comparably large in this type of geometric relationship. The following example is given to demonstrate the scenario where the L-CRLB is equal to CRLB.

Example 2 (Network Layout for Equivalent L-CRLB and CRLB) Assuming that the variances σ_{ri} from all the measurement noises are equivalent, the L-CRLB can achieve the CRLB if (a) the noiseless distances ζ_i from the MS to all the corresponding BSs are equal, and (b) the orientation angles α_i from the MS to all the BSs are uniformly distributed in [0°, 360°) as $\alpha_i = 360° \cdot (i-1)/N + \gamma$, $\forall \gamma = [0°, 360°)$ and $i = 1$ to N.

Proof By substituting the conditions $\zeta_1 = \zeta_2 = \ldots = \zeta_N$ and $\sigma_{r_1} = \sigma_{r_2} = \ldots = \sigma_{r_N}$ into (18), the necessary condition for the L-CRLB and the CRLB to be equivalent becomes $\sum_{i=1}^{N} \cos \alpha_i = 0$ and $\sum_{i=1}^{N} \sin \alpha_i = 0$. Based on the assumptions as stated above, an unit vector can be utilized to represent the distance from the MS to the ith BS as $v_i = [\cos \alpha_i, \sin \alpha_i]$ for $i = 1$ to N. In order to satisfy the conditions for both $\sum_{i=1}^{N} \cos \alpha_i = 0$ and $\sum_{i=1}^{N} \sin \alpha_i = 0$, the summation for projecting all unit vectors v_i for $i = 1$ to N on the x-axis and y-axis respectively should be equal to zero. In order to achieve this condition, it can be verified that the angles α_i will be uniformly distributed in [0°,360°) with its value equal to $\alpha_i = 360° \cdot (i-1)/N + \gamma$, $\forall \gamma = [0°, 360°)$. This completes the proof. □

Corollary 2 *The minimum L-CRLB ($\mathcal{C}_{L,m}$) is achieved if the conditions stated in (8) and (18) are satisfied.*

Proof It has been indicated that the minimum CRLB ($\mathcal{C}_m$) can be obtained if the conditions in (8) hold. Moreover, Corollary 1 proves that (18) should be satisfied for both L-CRLB and CRLB to be equivalent. Therefore, the minimum L-CRLB ($\mathcal{C}_{L,m}$) can be achieved if (8) and (18) are satisfied.

It can be observed from Corollary 2 that additional condition (18) should be satisfied for achieving minimum L-CRLB comparing with the minimum CRLB. The major difference is that the CRLB is affected by the angles α_i and signal variances σ_{ri}^2; while the L-CRLB additionally depends on the distance information ζ_i. Therefore, the performance of the L-LEP is affected by the additional relative distance information between the MS and BSs. In order to provide intuitive explanation, the exemplified network layout for achieving minimum L-CRLB is shown as follows.

Example 3 (Network Layout with Minimum L-CRLB) Following the requirement as in Lemmas 1 and 2 with $N = 3$ and all the variances are equivalent, i.e., $\sigma_{ri}^2 = \sigma_r^2$ for $i = 1$ to 3, and further assuming that the noiseless distances ζ_i from the MS to all the three BSs are equivalent, the minimum L-CRLB can be achieved only at the angle sets $\{\alpha_1, \alpha_2, \alpha_3\} = \{\gamma, \gamma + 120°, \gamma + 240°\}$ $\forall$ $\gamma = [0°, 360°)$.

Proof Considering $N = 3$ and $\sigma_{r\_1} = \sigma_{r\_2} = \sigma_{r\_3} = \sigma_r$ in (8), the following relationship is obtained:

$$\begin{cases} \sin 2\alpha_1 + \sin 2\alpha_2 + \sin 2\alpha_3 = 0 \\ \cos 2\alpha_1 + \cos 2\alpha_2 + \cos 2\alpha_3 = 0 \end{cases} \tag{19}$$

It can be verified that both conditions in (19) are only satisfied at either one of the following angle sets: $\{\alpha_1, \alpha_2, \alpha_3\} = \{\gamma, \gamma + 120°, \gamma + 240°\}$ and $\{\alpha_1, \alpha_2, \alpha_3\} = \{\gamma, \gamma + 60°, \gamma + 120°\}$ $\forall$ $\gamma = [0°, 360°)$. The corresponding minimum CRLB can be calculated from (7) as $\mathcal{C}_m = 4\sigma_r^2/3$.

On the other hand, according to Lemma 2, the conditions (8) and (18) must be satisfied in order to achieve minimum L-CRLB. Considering the $N = 3$ case with $\zeta_1 = \zeta_2 = \zeta_3$, condition (18) is rewritten as

$$\begin{cases} \sin\alpha_1 + \sin\alpha_2 + \sin\alpha_3 = 0 \\ \cos\alpha_1 + \cos\alpha_2 + \cos\alpha_3 = 0 \end{cases} \quad (20)$$

It can be verified that only the angle sets $\{\alpha_1, \alpha_2, \alpha_3\} = \{\gamma, \gamma + 120°, \gamma + 240°\}$ $\forall\ \gamma = [0°, 360°)$ can satisfy all the three conditions as defined in (19) and (20) for achieving the minimum value of L-CRLB. This completes the proof. □

In other words, when the MS is positioned at the center of a regular polygon formed by the BSs, the proposed L-CRLB will be equivalent to the CRLB based on the conditions stated in (18). Example 3 describes the fact that minimum CRLB can be achieved under two different set of orientation angles; while the minimum L-CRLB is reached by one of its subset of angles. This indicates the situation that the L-CRLB provides a more stringent criterion compared to the CRLB for achieving its minimum value. Even though certain network layouts are suggested to achieve minimum CRLB, it does not guarantee that the corresponding L-CRLB can reach the same value. Therefore, the CRLB does not provide sufficient information to be utilized as the criterion for the linearized location estimator of the L-LEP; while the L-CRLB can be more feasible to reveal the geometric properties and requirements.

In order to provide better explanation on the properties of CRLB and L-CRLB, the definitions of several geometric relationships between the MS and the BSs are described as follows.

Definition 5 (*BS's Adjacent Included Angle*) Based on the BS's orientation α_i, the adjacent included angle between two neighboring i-th and $(i + 1)$-th BSs is defined as $\beta_i = \alpha_{i+1} - \alpha_i$ for $i = 1$ to $N - 1$, and $\beta_N = 360° + \alpha_1 - \alpha_N$.

Definition 6 (*BS Polygon*) Considering the locations of BSs as the vertices in geometry, the BS polygon is defined by connecting the adjacent BSs as the edges of the polygon from BS_1 to BS_N.

Definition 7 (*Inside-Polygon Layout (IPL)*) Given the BS's adjacent included angle set $\boldsymbol{\beta} = \{\beta_1, \ldots, \beta_i, \ldots, \beta_N\}$, an inside-polygon layout (IPL) is defined if the MS is located inside the BS polygon where $0° < \beta_i < 180°$ $\forall$ i from 1 to N.

Definition 8 (*Outside-Polygon Layout (OPL)*) Given the BS's adjacent included angle set $\boldsymbol{\beta} = \{\beta_1, \ldots, \beta_i, \ldots, \beta_N\}$, a outside-polygon layout (OPL) is defined if the MS is located outside the BS polygon where there exists an adjacent included angle $180° \le \beta_i < 360°$ $\forall$ i from 1 to N.

Lemma 3 *Two types of layout, IPL and OPL, with equivalent variances* $\sigma^2_{r\_i,in} = \sigma^2_{r\_i,out}$ *and noiseless distances* $\zeta_{i,in} = \zeta_{i,out}$ *for* $i = 1$ *to* 3 *are considered between the MS and three BSs. There can exist* ***specific sets of IPL and OPL*** *that possess the same CRLB value; while the corresponding L-CRLB value of the IPL is smaller than that of OPL.*

Proof Given an IPL, the set of BS's adjacent included angle is defined as $\boldsymbol{\beta}_{in} = \{\beta_1, \beta_2, \beta_3 = 360° - \beta_1 - \beta_2\}$ where $0° < \beta_i < 180°$ $\forall$ $i = 1$ to 3. The set of BS's orientation between the MS and three BSs can be represented as $\boldsymbol{\alpha}_{in} = \{\alpha_1 = 0, \alpha_2 = \beta_1, \alpha_3 = \beta_1 + \beta_2\}$. Without lose of generality, α_1 is set with zero degree according to the rotation property as proven in [19] for CRLB. In order to establish an OPL, the third BS is repositioned to the reflected side with respect to the MS, which results in its BS's orientation as $\boldsymbol{\alpha}_{out} = \{\alpha_1 = 0, \alpha_2 = \beta_1, \alpha'_3 = \beta_1 + \beta_2 - 180°\}$. By substituting both IPL and OPL cases with $\boldsymbol{\alpha}_{in} = \{0, \alpha_2, \alpha_3\}$ and $\boldsymbol{\alpha}_{out} = \{0, \alpha_2, \alpha_3 - 180°\}$ respectively into (3), it can be observed that same value of CRLB is achieved by both IPL and OPL.

Moreover, in order to compare the L-CRLB for the IPL and OPL, i.e., $\mathcal{C}_{L,in}$ and $\mathcal{C}_{L,out}$, the difference of L-CRLB for both layouts is derived from (13) to (15) with the substitution of $\boldsymbol{\alpha}_{in}$ and $\boldsymbol{\alpha}_{out}$ as

$$\begin{aligned} \delta &= \mathcal{C}_{L,in} - \mathcal{C}_{L,out} = [\mathbf{I}_{\theta,in}]^{-1}_{11} + [\mathbf{I}_{\theta,in}]^{-1}_{22} - [\mathbf{I}_{\theta,out}]^{-1}_{11} - [\mathbf{I}_{\theta,out}]^{-1}_{22} \\ &= \frac{1}{D_{\mathbf{I}_{\theta,in}} D_{\mathbf{I}_{\theta,out}}} \left\{ -8\cos\frac{\alpha_2}{2}\cos\frac{2\alpha_3 - \alpha_2}{2}(1 - \cos\alpha_2)[2\cos\alpha_2 + 2\cos\alpha_3\cos(\alpha_2 - \alpha_3) - 4] \right\} \end{aligned} \quad (21)$$

where $D_{\mathbf{I}\theta,in}$ and $D_{\mathbf{I}\theta,out}$ denote the determinants of the FIM matrix $\mathbf{I}_{\theta,in}$ and $\mathbf{I}_{\theta,\ out}$ for the L-CRLB of IPL and OPL respectively. Since both $\mathbf{I}_{\theta,in}$ and $\mathbf{I}_{\theta,\ out}$ are positive definite, their corresponding determinants $D_{\mathbf{I}\theta,in}$ and $D_{\mathbf{I}\theta,out}$ will be positive values. Furthermore, the following conditions hold since the BS's orientation set $\boldsymbol{\alpha}_{in}$ corresponds to an IPL: $0° < \alpha_2 < 180°$, $0° < \alpha_3 - \alpha_2 < 180°$, and $180° < \alpha_3 < 360°$. Therefore, the following conditions hold for the numerator terms in (21): $\cos(\alpha_2/2) > 0$ since $0° < \alpha_2/2 < 90°$, $\cos[(2\alpha_3 - \alpha_2)/2] < 0$ since $90° < (2\alpha_3 - \alpha_2)/2 < 270°$, $(1 - \cos\alpha_2) > 0$ since $-1 < \cos\alpha_2 < 1$, and $2\cos\alpha_2 + 2\cos\alpha_3\cos(\alpha_2 - \alpha_3) < 4$ since $-1 < \cos\alpha_2 < 1$ and $-1 < \cos\alpha_3\cos(\alpha_2 - \alpha_3) < 1$. As a consequence, the difference

$\delta = \mathcal{C}_{L,in} - \mathcal{C}_{L,out} < 0$ which corresponds to the result that the L-CRLB of the IPL is smaller than that of the OPL. This completes the proof. □

Lemma 3 limits the discussion to a specific MS set, i.e., the positions of MS that can achieve the same CRLB given the same set of BSs. A key contribution of this paper is obtained from Lemma 3 that the proposed L-CRLB can distinguish different geometric relationships between the MS and its corresponding BSs, i.e., either the IPL or OPL; while the conventional CRLB criterion observes the same value for both cases. It is proved in Lemma 3 that the L-CRLB for MS to locate inside the BS polygon will be smaller than that for MS situated outside the BS polygon. This result implicitly indicates that the estimation accuracy from a linearized location estimator will be higher for the IPL compared to the OPL case in general. The conjecture to possess higher estimation precision for the IPL compared to that for the OPL will be validated via simulations in Sect. 4.

3 LLS formulation

Note that the LLS method is proposed to solve the L-LEP instead of the conventional LEP. By combining (1) and (2) within the LS formulation, the following matrix format can be acquired:

$$\mathbf{M}\boldsymbol{\theta} = \mathbf{J} \tag{22}$$

where

$$\mathbf{M} = \begin{bmatrix} -2x_1 & -2y_1 & 1 \\ -2x_2 & -2y_2 & 1 \\ . & . & . \\ -2x_N & -2y_N & 1 \end{bmatrix} \qquad \mathbf{J} = \begin{bmatrix} r_1^2 - \kappa_1 \\ r_2^2 - \kappa_2 \\ . \\ r_N^2 - \kappa_N \end{bmatrix}$$

where $\kappa_i = x_i^2 + y_i^2$. Based on (22), the MS's estimated position by adopting the LLS method (i.e., $\hat{\boldsymbol{x}}_{LLS} = [\hat{x}_{LLS}, \hat{y}_{LLS}]^T$) can be acquired as

$$\hat{\boldsymbol{x}}_{LLS} = \mathbf{P}(\mathbf{M}^T\mathbf{M})^{-1}\mathbf{M}^T\mathbf{J} \tag{23}$$

where $\mathbf{P} = [1\ 0\ 0;\ 0\ 1\ 0]$. As observed from the difference between the L-CRLB and the conventional CRLB in Sect. 2, the additional nonlinear parameter R prevents the LLS to approach the CRLB. However, the LLS method can approach the L-CRLB well under the Gaussian Noise assumption. Note that both the CRLB and the L-CRLB represent lower bounds for unbiased estimators. Therefore, the target of this following lemma is to identify the conditions for the unbiased properties to be satisfied associated with the LLS location estimator based on TOA signals.

Lemma 4 *The LLS estimator is an unbiased estimator for the location estimation providing that all the TOA measurements are line-of-sight (LOS) signals and the corresponding noiseless distance is much greater than the combined noise for each measurement.*

Proof The primary concern of this proof is to acquire the expected value of estimation error $\Delta\hat{\boldsymbol{x}}_{LLS} = [\Delta\hat{x}_{LLS}, \Delta\hat{y}_{LLS}]^T$, which can be obtained by rewriting (23) as

$$\Delta\hat{\boldsymbol{x}}_{LLS} = \mathbf{P} \cdot (\mathbf{M}^T\mathbf{M})^{-1}\mathbf{M}^T\Delta\mathbf{J} \tag{24}$$

It is noted that (24) indicates that the estimation error vector $\Delta\hat{\boldsymbol{x}}_{LLS}$ is incurred by the variation within the vector $\mathbf{J}$. The value of $\Delta\mathbf{J}$ is obtained by considering the variations from the measurement inputs, i.e., $r_i = \zeta_i + n_i$ in (1), with $N = 3$ case as

$$\Delta\mathbf{J} = \begin{bmatrix} 2\zeta_1 n_1 + (n_1)^2 \\ 2\zeta_2 n_2 + (n_2)^2 \\ 2\zeta_3 n_3 + (n_3)^2 \end{bmatrix} \simeq \begin{bmatrix} 2\zeta_1 n_1 \\ 2\zeta_2 n_2 \\ 2\zeta_3 n_3 \end{bmatrix} \tag{25}$$

It is noted that the approximation from the second equality within (25) is valid by considering that the noiseless distance ζ_i is in general much greater than the combined noise effect n_i in practice, i.e., $\zeta_i > > n_i$. Without lose of generality, coordinate transformation can be adopted within (24) such that $(x_1, y_1) = (0, 0)$. The expected value of estimation error can therefore be acquired by expanding (24) as

$$\begin{aligned} E[\Delta\hat{x}_{LLS}] &= E\left[\frac{\zeta_3 n_3 y_2 - \zeta_2 n_2 y_3 - \zeta_1 n_1 (y_3 - y_2)}{x_2 y_3 - x_3 y_2}\right] \\ &= \frac{\zeta_3 y_2 \cdot E[n_3] - \zeta_2 y_3 \cdot E[n_2] - \zeta_1 (y_3 - y_2) \cdot E[n_1]}{x_2 y_3 - x_3 y_2} \end{aligned} \tag{26}$$

$$\begin{aligned} E[\Delta\hat{y}_{LLS}] &= E\left[\frac{\zeta_3 n_3 x_2 - \zeta_2 n_2 x_3 - \zeta_1 n_1 (x_3 - x_2)}{x_2 y_3 - x_3 y_2}\right] \\ &= \frac{\zeta_3 x_2 \cdot E[n_3] - \zeta_2 x_3 \cdot E[n_2] - \zeta_1 (x_3 - x_2) \cdot E[n_1]}{x_2 y_3 - x_3 y_2} \end{aligned} \tag{27}$$

From (26) and (27), it can be clearly observed that the expected value of estimation error is zero under the assumption that its associated measurement are considered LOS signals as zero mean random variables, i.e., $E[n_i] = 0 \ \ \forall\ i$. This completes the proof. □

Lemma 4 reveals the fact that the LLS estimator can be regarded as an unbiased estimator under the condition $\zeta_i > > n_i$, which is considered reasonable in practice. Since the L-CRLB represents the theoretical lower bound for any unbiased estimator in the L-LEP, it can therefore be utilized as the lower bound for the LLS estimator. Moreover, the mean square error of LLS estimator can also be

derived from (26) and (27) under the situation that the measurement noises are independent with each other, i.e., $E[n_i \cdot n_j] = 0 \, \forall i \neq j$, which is obtained as follows:

$$E[\Delta\hat{x}_{LS}^2] = \frac{\zeta_2^2 y_3^2 \sigma_{n_2}^2 + \zeta_3^2 y_2^2 \sigma_{n_3}^2 + \zeta_1^2 (y_3 - y_2)^2 \sigma_{n_1}^2}{(x_3 y_2 - x_2 y_3)^2} \tag{28}$$

$$E[\Delta\hat{y}_{LS}^2] = \frac{\zeta_2^2 x_3^2 \sigma_{n_2}^2 + \zeta_3^2 x_2^2 \sigma_{n_3}^2 + \zeta_1^2 (x_3 - x_2)^2 \sigma_{n_1}^2}{(x_3 y_2 - x_2 y_3)^2} \tag{29}$$

Noted that (28) and (29) are also derived based on the condition that $\zeta_i >> n_i$. Meanwhile, it is interesting to notice that the variance of LLS estimator calculated from (28) and (29) will be numerically identical to the L-CRLB computed via (13), which will be validated and shown in the following section. Therefore, the LLS estimator will approach its defined lower bound L-CRLB under the situation with smaller measurement noises. Furthermore, the L-CRLB will become the conventional CRLB under specific geometric layout as described in Corollary 1. As a result, under specific conditions as stated above, the LLS estimator can be claimed as the best estimator since it can finally reach the theoretical lower bound, i.e., CRLB, for unbiased estimators.

4 Performance evaluation

In order to verify the effectiveness of L-CRLB derived in Sect. 2.3, different scenarios are provided in the section to validate the correctness of the formulation. The model for the measurement noise of TOA signal n_i as in (1) is selected as the Gaussian distribution with zero mean and standard deviation σ_{r_i}, i.e., $n_i \sim \mathcal{N}(0, \sigma_{r_i}^2)$. Section 4.1 presents the contour plots in order to numerically describe the difference between the CRLB and L-CRLB, which also validate the correctness of Lemmas 1 to 2 and Corollaries 1 to 2. Section 4.2 simulates the performance of LLS method by comparing the L-CRLB and LLS estimator in the regular BS polygon layout. Section 4.3 illustrates the performance comparison of LLS estimator under both the IPL and OPL cases. Performance comparison under realistic WSN scenario is described in Sect. 4.4.

4.1 Numerical validation of CRLB and L-CRLB with a regular triangular layout

In order to observe the difference between the CRLB and L-CRLB, their corresponding contour plots under the number of BSs $N = 3$ are shown in Fig. 1(a) and (b), respectively. Note that the three BSs are located at the vertexes of a regular triangular which are denoted with red circles in Fig. 1(a) and (b). The positions of BSs are $\boldsymbol{x}_1 = [300, 200]^T$ with $\alpha_1 = 0°, \boldsymbol{x}_2 = [150, 286.6]^T$ with $\alpha_2 = 120°$, and $\boldsymbol{x}_3 = [150, 113.4]^T$ with $\alpha_3 = 240°$. Based on the three BS's positions, each individual contour point represents the corresponding CRLB or L-CRLB value when the MS is situated at that geographical location. The standard deviation of measurement noises σ_{r_i} is chosen as 1 m for simplicity. It can be observed from Fig. 1(a) that there are four minimum points for the CRLB value equal to $\mathcal{C}_m = 1.33$ with MS's positions as $\boldsymbol{x} = [200, 200]^T, [100, 200]^T, [260, 120]^T$, and $[260,280]^T$. The conditions for minimum CRLB can be verified by substituting the corresponding parameters into the condition (8). The minimum CRLB value can also be validated to satisfy (7), which demonstrates the correctness of Lemma 1.

On the other hand, by comparing Fig. 1(a) and (b), it is observed that the distribution of L-CRLB is different from that of CRLB. The only minimum L-CRLB value identical to that of the CRLB, i.e., $\mathcal{C}_{L,m} = \mathcal{C}_m = 1.33$, is located at the center of regular triangle formed by the three BSs, i.e., $\boldsymbol{x} = [200, 200]^T$. Starting at the MS's position with minimum L-CRLB, the L-CRLB value will increase in all directions. Except for the minimum L-CRLB at the center of the triangle, the relationship that $\mathcal{C}_L > \mathcal{C}$ can be observed from both Fig. 1(a) and (b). Moreover, the difference between the L-CRLB and CRLB inside the triangle is

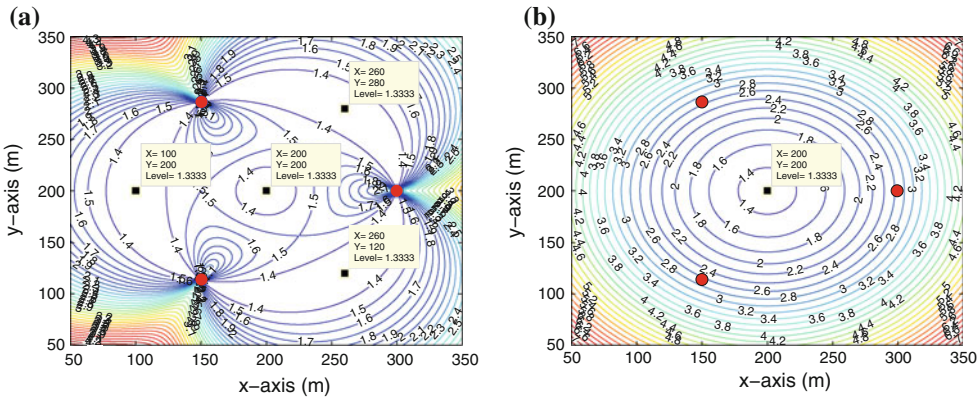

Fig. 1 **a** CRLB contour under $N = 3$; **b** L-CRLB contour under $N = 3$. *Red circles* denote the positions of BSs (Color figure online)

smaller than that outside of the triangle. The reason can be contributed to the estimation of parameter R by adopting the L-CRLB criterion, which introduces the two terms ε_1 and ε_2. Owing to the nonlinear behavior of location estimation, the additional consideration of R within the L-CRLB can better characterize the performance of linearized location estimator for the L-LEP. The correctness of minimum L-CRLB value obtained from Fig. 1(b) can also be verified by substituting corresponding parameters into the conditions stated in Lemma 2, i.e., the conditions (8) and (18) can all be satisfied. By comparing the results from Fig. 1(a) and (b), Corollaries 1 to 2 and Examples 2 to 3 can all be validated by substituting the corresponding numerical values.

4.2 Performance validation of LLS estimator with a regular BS polygon layout

In this subsection, the performance of LLS estimator is simulated to further validate the relationship between the estimator and the lower bound. Figure 2 illustrates the performance comparison under different noise standard deviations in the regular triangular layout, i.e., $N = 3$. The coordinates of the 3 BSs are listed in the 3 BS case of Table 1, and the MS is located at the coordinate $\boldsymbol{x} = [200, 200]^T$. Moreover, Fig. 3 shows the performance comparison between different numbers BSs of regular BS polygon layout where the MS lies at $\boldsymbol{x} = [200, 200]^T$ and the standard deviation of measurement noise is equal to 10 m. The BS's coordinates correspond to different numbers of BSs' layout are listed in Table 1. Regarding the comparison metrics, instead of showing the variances, the root mean square error (RMSE) is obtained in order to clearly illustrate the difference between different curves, i.e., $\mathrm{RMSE} = \left[\sum_{i=1}^{N_r} \|\boldsymbol{x} - \hat{\boldsymbol{x}}(i)\|^2 / N_r\right]^{1/2}$, where $N_r = 10{,}000$ indicates the number of simulation runs. As for the curves within Figs. 2 and 3, the LLS estimator denotes the RMSE of $\hat{\boldsymbol{x}}_{LLS}$ acquired from (23) by simulating the Gaussian noises with corresponding noise standard deviations. Since the CRLB and the L-CRLB represent the variance of an unbiased estimator, both the CRLB and L-CRLB curves are obtained by taking the square root in order to compared with the RMSE values of LLS estimator. Furthermore, the curve of LLS standard deviation in Fig. 2 is obtained as the square root of LLS variance derived from (28) and (29).

It can be observed from Fig. 2 that the CRLB, L-CRLB, and LLS standard deviation can achieve the same values in the regular triangular layout. The reason for the CRLB and L-CRLB to possess the same value is identical to the

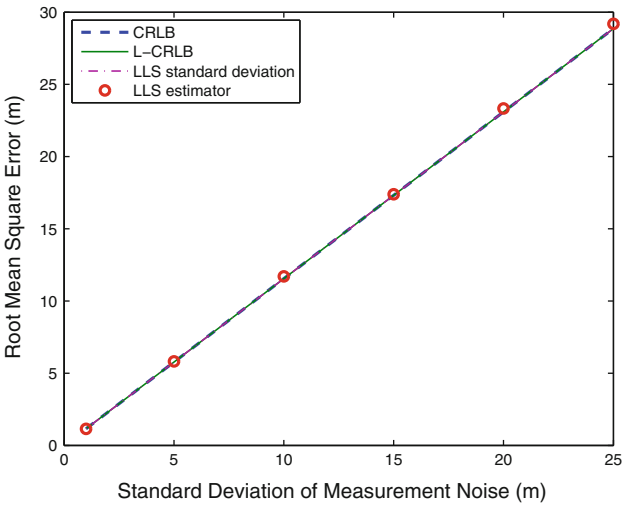

Fig. 2 Performance comparison for location estimation with MS at the center of a regular triangle formed by 3 BSs as listed in Table 1: RMSE versus standard deviation of measurement noise. The CRLB, L-CRLB, and LLS standard deviation achieve the same values

Table 1 Simulation parameters

Number of BSs	i-th BS's Coordinate x_i in meter		
3 BSs	0°: $[300,200]^T$	120°: $[150,286.6]^T$	240°: $[150,113.4]^T$
4 BSs	0°: $[300,200]^T$	90°: $[200,300]^T$	180°: $[100,200]^T$
	270°: $[200,100]^T$		
5 BSs	0°: $[300,200]^T$	72°: $[230.9,295.1]^T$	144°: $[119.1,258.8]^T$
	216°: $[119.1,141.2]^T$	288°: $[230.9,104.9]^T$	
6 BSs	0°: $[300,200]^T$	60°: $[250,286.6]^T$	120°: $[150,286.6]^T$
	180°: $[100,200]^T$	240°: $[150,113.4]^T$	300°: $[250,113.4]^T$
7 BSs	0°: $[300,200]^T$	51.4°: $[262.3,278.2]^T$	102.8°: $[177.7,297.5]^T$
	154.3°: $[109.9,243.4]^T$	205.7°: $[109.9,156.6]^T$	257.1°: $[177.7,102.5]^T$
	308.6°: $[262.3,121.8]^T$		
8 BSs	0°: $[300,200]^T$	45°: $[270.7,270.7]^T$	90°: $[200,300]^T$
	135°: $[129.3,270.7]^T$	180°: $[100,200]^T$	225°: $[129.3,129.3]^T$
	270°: $[200,100]^T$	315°: $[270.7,129.3]^T$	

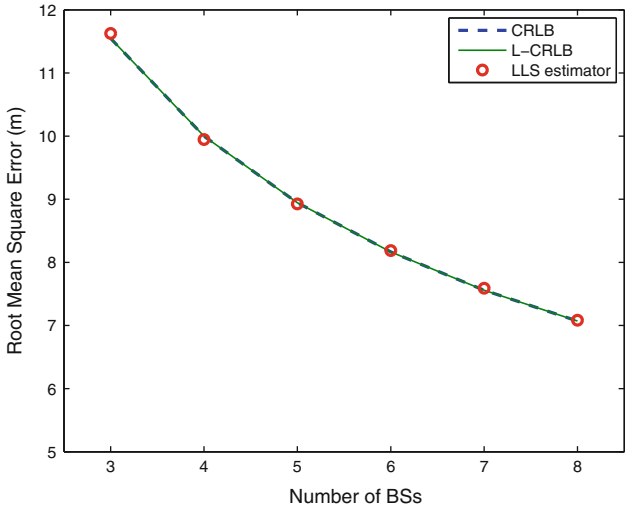

Fig. 3 Performance comparison for location estimation with MS at the center of a regular BS polygon formed by the BSs as listed in Table 1: RMSE versus the number of BSs. The standard deviation of measurement noise is 10 m. The CRLB and L-CRLB achieve the same values

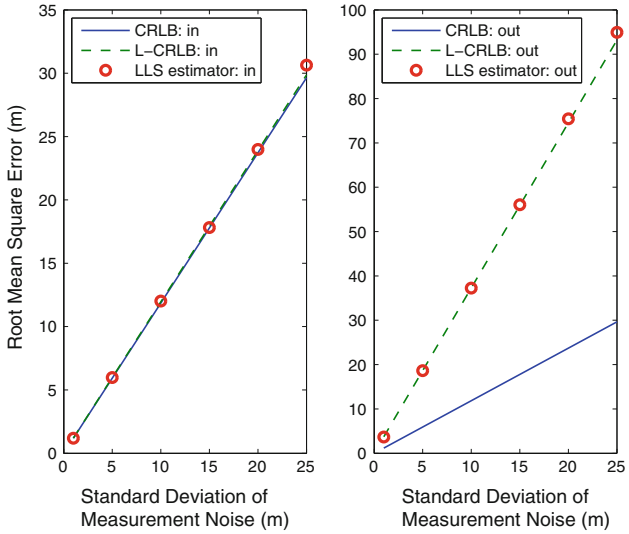

Fig. 4 Performance comparison for location estimation under 3 BSs triangular layout: RMSE versus standard deviation of measurement noise. *Left plot* the MS is located inside the triangle formed by BSs; *Right plot* the MS is outside of the triangle formed by BSs. The CRLB values are the same in both plots

conditions as stated in Lemmas 1 and 2. As described in Sect. 3, the LLS standard deviation is numerically validated in this figure to be identical to the square roots of CRLB and L-CRLB under the condition $\zeta_i >> n_i$. The performance of LLS estimator obtained from simulations can also approach both lower bounds, i.e., the CRLB and L-CRLB, under the cases with smaller measurement noises. This result demonstrates that the LLS estimator can be considered as an efficient estimator for the LEP and L-LEP under smaller measurement noises. On the other hand, as the noise becomes larger which disobeys the relationship $\zeta_i >> n_i$, it is observed that the RMSE of LLS estimator will be slightly higher than that obtained from the L-CRLB.

Figure 3 validates the performance of LLS estimator in the regular BS polygon layouts under different numbers of BSs. In order to observe the difference between the LLS estimator and the L-CRLB, the error confidential level (δ) is defined as the difference between the RMSE of LLS estimator ($\mathcal{R}_{LLS}$) and the square root of L-CRLB ($\mathcal{R}_L$), i.e., $\delta = |\mathcal{R}_{LLS} - \mathcal{R}_L|/\mathcal{R}_L$. In Fig. 3, the error confidential levels can be obtained as $\delta = [0.67, 0.53, 0.20, 0.27, 0.41, 0.17]$ % under the number of BSs equal to [3–8]. It is observed that the LLS estimator can closely approach both of the lower bounds CRLB and L-CRLB under different numbers of available BSs.

4.3 Performance comparison of LLS estimation with IPL and OPL

In the subsection, the IPL and OPL which achieve the same CRLB value are adopted to validate the correctness of Lemma 3. The MS is placed at the position $\boldsymbol{x} = [200, 200]^T$ m, and the distances from all the BSs to the MS are designed to be equal to 100 m. The angle set for the IPL is assigned as {0°, 70°, 240°}, and that for the OPL is {0°, 60°, 70°}. That is, the three BSs of IPL is placed at $[300, 200]^T$, $[234.2, 294]^T$, and $[150,113.4]^T$, and that for the OPL is located at $[300, 200]^T$, $[250, 286.6]^T$, and $[234.2,294]^T$. It is noted that the square roots of CRLB for both the IPL and the OPL are obtained to have the same value as 1.34.

The left subplot of Fig. 4 shows the performance of LLS estimator comparing with both CRLB and L-CRLB under the IPL; while the right subplot of Fig. 4 corresponds to that for the OPL. In order to clearly show the difference between these curves, different scales are utilized in both plots. It can be observed that the performance of LLS estimator still matches that of the L-CRLB under the cases with smaller measurement noises for both plots, which again shows that the L-CRLB can closely characterize the behaviors of LLS estimator. However, the difference between the L-CRLB and the CRLB in the OPL is comparably larger than the IPL case, which validates the correctness of Lemma 3. Therefore, it is concluded that the LLS estimator can provide better performance in the IPL compared to the OPL even though both layouts result in same value of CRLB.

4.4 Performance comparison of LLS estimation in a WSN scenario

In order to consider more realistic environments, Fig. 5 illustrates the simulation scenarios of a WSN with a grid-

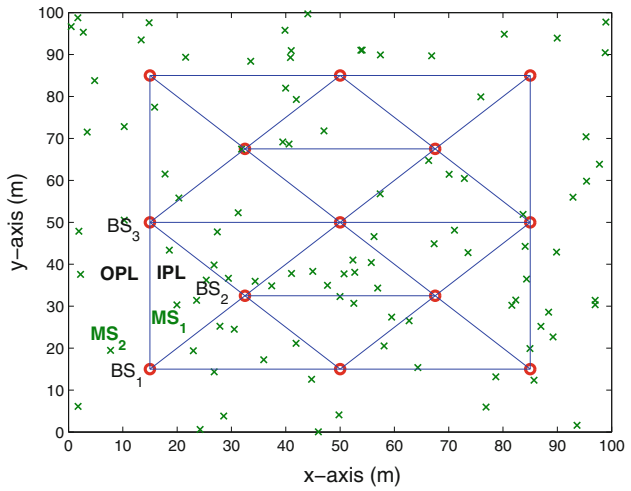

Fig. 5 Layout of the WSN scenario: *red circles* represent the positions of anchor BSs and *green crosses* denote the positions of MS (Color figure online)

based placement for the coordinates of both MSs and BSs. There are total 13 BSs (denoted by red circles) and the MS's positions (denoted by green crosses) are placed at 100 different locations uniformly distributed in a two-dimensional 100 m × 100 m rectangular region. The MS selects the closest BSs and estimates its position upon receiving the distance measurements from those selected BSs. As will be shown in Fig. 6, the number of BSs are selected from three to eight respectively for performance comparison. According to the random deployment of

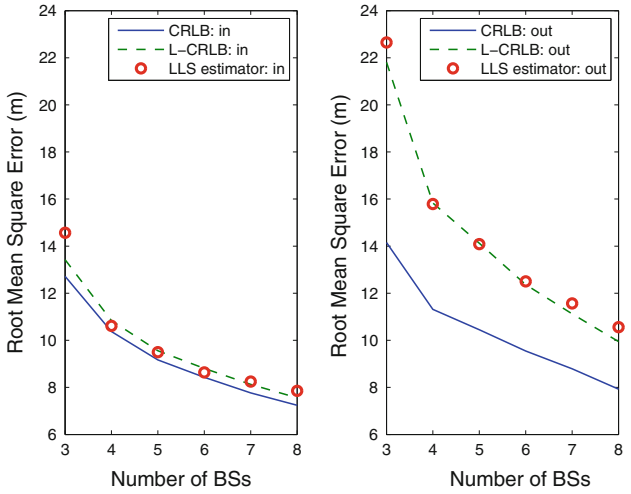

Fig. 6 Performance comparison for location estimation with uniformly distributed MS and the BS's coordinates in Fig. 5: RMSE versus number of BSs. The standard deviation of measurement noise is 10 m. *Left plot* the MS is located inside the BS polygon; *Right plot* the MS is situated outside of the BS polygon

MSs, it is intuitive that some MSs will be located in IPL and the others are in OPL. In order to clearly illustrate either inside or outside polygon in a grid-based placement in Fig. 5, the network layout is partitioned into triangular regions by connecting the BSs with blue lines considering the case that the required number of BSs is equal to three. The MSs within each triangular area will connect to the BSs located at the three vertexes since those are the three closest BSs to the MSs. For example, as shown in Fig. 5, MS_1 is classified into IPL since it is located inside the BS polygon, i.e., the triangular area, connected by BS_1, BS_2, and BS_3. On the other hand, MS_2 belongs to OPL owing to the reason that it is located outside of the triangular region formed by the three closest BSs, i.e., BS_1, BS_2, and BS_3.

Based on the grid-based WSN setup, Fig. 6 shows the performance evaluation of LLS estimator in comparison with both CRLB and L-CRLB under different numbers of received BSs with IPL and OPL cases in the left and right subplots, respectively. For either IPL or OPL cases, the RMSE is computed to include all the MSs classified in either IPL or OPL respectively, i.e., RMSE $= \left[\sum_{j=1}^{N_I}\sum_{i=1}^{N_r}\|\boldsymbol{x}_j-\hat{\boldsymbol{x}}_j(i)\|^2/(N_r\cdot N_I)\right]^{1/2}$, where $N_r = 1{,}000$ indicates the number of simulation runs and N_I represents the number of MSs in either IPL or OPL. Both the CRLB and L-CRLB are also obtained by averaging the corresponding values from different MS's positions. Therefore, the simulations can represent average estimation results for a grid-based WSN scenarios under either IPL or OPL case. Comparing with the CRLB, it is observed that the proposed L-CRLB can better characterize the simulation results for LLS estimator under both the IPL and OPL cases. Moreover, the LLS estimator can still provide better performance within the IPL in comparison with that in the OPL. This conclusion is both validated via theoretical proof in Lemma 3 and simulation results in Fig. 5. Furthermore, the LLS performance under the IPL can be similar to that under the OPL which utilizes additional measurement input. For example, as shown in Fig. 5, the RMSE of the 4 BSs case under the IPL can be obtained as 10.7 m; while the RMSE of the 5 BSs case under the OPL is 10.65 m. However, additional number of BSs utilized in a location estimate requires more communication overheads.

Since the multi-path, delay, and small fading are location-dependent, different noise settings within the same network layout in Fig. 5 are utilized to discuss the effect from measurement noises. Instead of considering a single standard deviation of measurement noise as 10 m, the standard deviation of measurement noise σ_n is designed to be uniformly sampled from [0, 20], i.e., $\sigma_n \sim U[0,20]$. The left and right plots of Fig. 7 illustrate the RMSE

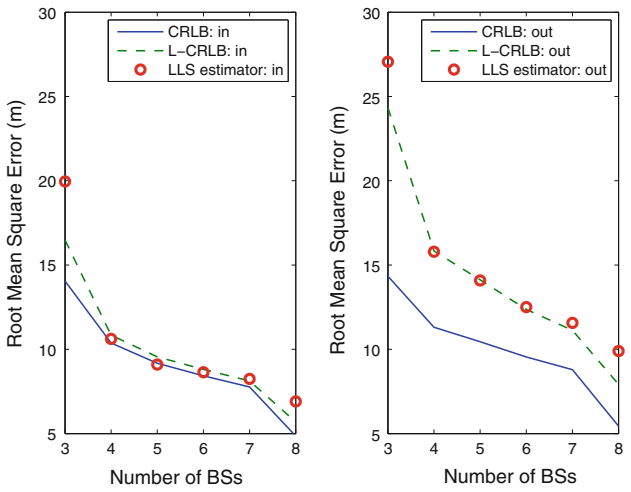

Fig. 7 Performance comparison for location estimation with uniformly distributed MS and the BS's coordinates in Fig. 5: RMSE versus number of BSs. The standard deviation of measurement noise is uniformly distribution as $U[0, 20]$. *Left plot* the MS is located inside the BS polygon; *Right plot* the MS is situated outside of the BS polygon

performance of MSs in IPL and OPL, respectively. The measured relative distance between the MS and BS in (1) can be generated based on σ_n since $n_i \sim \mathcal{N}(0, \sigma_n^2)$. With the consideration of various levels of measurement noise, it can be observed that the LLS estimator with weighted matrix obtained from noise standard deviation can still approach the L-CRLB in both IPL and OPL cases. As a consequence, from the study of geometric effect of LLS estimator, it is suggested that the OPL should be avoided in order to increase the precision of MS's location estimation. This conclusion will be valuable for either cellular networks or WSNs while either conducting the deployment of BSs or implementing a BS selection algorithm.

5 Conclusion

This paper derives the linearized location estimation problem based Cramèr-Rao lower bound (L-CRLB) which provides the analytical form to discuss the geometric effect for the linear least square (LLS) estimator. The geometric properties and the relationships between the L-CRLB and conventional CRLB are obtained with theoretical proofs. It is validated in the simulations that the L-CRLB can provide the tight lower bound for the LLS estimator, especially under the situations with smaller measurement noises. Moreover, the proposed L-CRLB can be utilized to describe the performance difference of an LLS estimator under different geometric layouts. The MS locates inside a BS-constrained geometry will provide higher estimation accuracy comparing with the case that the MS is situated outside of the BS-confined geometry layout.

Acknowledgments This work was in part funded by the Aiming for the Top University and Elite Research Center Development Plan, NSC 99-2628-E-009-005, the MediaTek research center at National Chiao Tung University, and the Telecommunication Laboratories at Chunghwa Telecom Co. Ltd, Taiwan.

References

1. *Enhanced 911–Wireless Services*. Federal Communication Commission. [Online]. Available: http://www.fcc.gov/pshs/services/911-services (visit on Feb. 2010).
2. Patwari, N., Ash, J. N., Kyperountas, S., Hero, III A. O., Moses, R. L., & Correal, N. S. (2005). Locating the nodes: Cooperative localization in wireless sensor networks. *IEEE Signal Processing Magazine, 22*, 54–69.
3. Gezici, S., Tian, Z., Giannakis, G. B., Kobayashi, H., Molisch, A. F., Poor, H. V. et al. (2005). Localization via Ultra-wideband radios: A look at positioning aspects for future sensor networks. *IEEE Signal Processing Magazine, 22*, 70–84.
4. Hara, S., Zhao, D., Yanagihara, K., Taketsugu, J., Fukui, K., Fukunaga, S. et al. (2005). Propagation characteristics of IEEE 802.15.4 radio signal and their application for location estimation. In *IEEE Vehicular Technology Conference*, pp. 97–101.
5. Feng, S., & Law, C. L. (2002) Assisted GPS and Its Impact on Navigation in Intelligent Transportation Systems. In: *IEEE Intelligent Transportation Systems*, 926–931.
6. Farradyne, P. (2005). *Vehicle infrastructure integration (VII)—architecture and functional requirements*, draft version 1.0 ed.
7. Perusco, L., & Michael, K. (2007). Control, trust, privacy, and security: Evaluating location-based services. *IEEE Technology and Society Magazine, 26*, 4–16.
8. Zhao, Y. (2002). Standardization of mobile phone positioning for 3G systems. *IEEE Communications Magazine, 40*, 108–116.
9. Sayed, A. H., Tarighat, A., Khajehnouri, N. (2005). Network-based wireless location: Challenges faced in developing techniques for accurate wireless location information. *IEEE Signal Processing Magazine, 22*, 25–40.
10. Foy, W. H. (1976). Position-location solutions by Taylor-series estimation. *IEEE Transactions on Aerospace and Electronic Systems, 12*, 187–194.
11. Bahl, P., & Padmanabhan, V. N. (2000). RADAR: An in-building RF-based user location and tracking system. In *IEEE INFOCOM*, pp. 775 –784.
12. Caffery, Jr. J. J. (2000). A new approach to the geometry of TOA location. In *IEEE Proceedings of vehicular technology Conference*, pp. 1943–1949.
13. Priyantha, N. B. (2005). *The cricket indoor location system*. Ph.D. dissertation, Massachusetts Institute of Technology.
14. Cheung, K. W., So, H. C., Ma, W. K., & Chan, Y. T. (2004). Least squares algorithms for time-of-arrival-based mobile location. *IEEE Transactions on Signal Processing, 52*, 1121–1128.
15. Wei, H.-W., Wan, Q., Chen, Z.-X., & Ye, S.-F. (2008). A novel weighted multidimensional scaling analysis for time-of-arrival-based mobile location. *IEEE Transactions on Signal Processing, 56*, 3018–3022.

16. Yu, K. (2007). 3-D localization error analysis in wireless networks. *IEEE Transactions on Wireless Communications, 6*, 3473–3481.
17. Tseng, P.-H., & Feng, K.-T. (2009). Hybrid Network/satellite-based location estimation and tracking systems for wireless networks. *IEEE Transactions on Vehicular Technology, 58*(9), 5174–5189.
18. Chaffee, J., & Abel, J. (1994). GDOP and the Cramer-Rao bound. In *IEEE position location and navigation system (PLANS) conference*, pp. 663–668.
19. Chang, C., & Sahai, A. (2004). Estimation bounds for localization. In: *IEEE Sensor and Ad Hoc Communications and Networks (SECON)*, pp. 415–424.
20. Kay, Steven M. (1993). *Fundamentals of statistical signal processing: Estimation theory*. USA: Prentice Hall.

Author Biographies

Po-Hsuan Tseng received the B.S. and Ph.D. degrees in communication engineering from the National Chiao Tung University, Hsinchu, Taiwan, in 2005 and 2011, respectively. From January 2010 to October 2010, he was a Visiting Researcher with the University of California at Davis. His research interests are in the areas of signal processing for networking and communications, including location estimation and tracking, cooperative localization, and mobile broadband wireless access system design.

Kai-Ten Feng received the B.S. degree from the National Taiwan University, Taipei, Taiwan, in 1992, the M.S. degree from the University of Michigan, Ann Arbor, in 1996, and the Ph.D. degree from the University of California, Berkeley, in 2000. Between 2000 and 2003, he was an In-Vehicle Development Manager/Senior Technologist with OnStar Corporation, a subsidiary of General Motors Corporation, where he worked on the design of future Telematics platforms and in-vehicle networks. Since August 2011, he has been a full Professor with the Department of Electrical Engineering, National Chiao Tung University (NCTU), Hsinchu, Taiwan, where he was an Associate Professor and Assistant Professor from August 2007 to July 2011 and from February 2003 to July 2007, respectively. From July 2009 to March 2010, he was a Visiting Scholar with the Department of Electrical and Computer Engineering, University of California at Davis. He has also been the Convener of the NCTU Leadership Development Program since August 2011. Since October 2011, he has been serving as the Director of the Digital Content Production Center at the same university. His current research interests include broadband wireless networks, cooperative and cognitive networks, smart phone and embedded system designs, wireless location technologies, and intelligent transportation systems. Dr. Feng received the Best Paper Award from the Spring 2006 IEEE Vehicular Technology Conference, which ranked his paper first among the 615 accepted papers. He also received the Outstanding Youth Electrical Engineer Award in 2007 from the Chinese Institute of Electrical Engineering and the Distinguished Researcher Award from NCTU in 2008, 2010, and 2011. He has served on the technical program committees of the Vehicular Technology, International Communications, and Wireless Communications and Networking Conferences.